communications earth & environment

ARTICLE

https://doi.org/10.1038/s43247-023-00974-4 OPEN

Moon's high-energy giant-impact origin and differentiation timeline inferred from Ca and Mg stable isotopes

Hairuo Fu [1]✉, Stein B. Jacobsen[1] & Fatemeh Sedaghatpour[1]

Mass-dependent stable isotopic variations recorded in lunar samples provide novel resolution to the formation and differentiation history of the Moon. In this study, we report new high-precision Ca-isotope measurements for lunar rocks and minerals. Ca-isotope data and modeling of the lunar magma ocean together demonstrate indistinguishable mass-dependent Ca isotopic compositions of the bulk silicate Earth and Moon. This implied Earth-Moon isotope equilibration is consistent with the Moon's high-energy giant-impact (Synestia) origin and not readily compatible with the traditional giant-impact models. Moreover, a cross-comparison between Ca and Mg isotopic data for an important anorthosite sample (60025) consistently clarifies its formation near the completion of the lunar magma ocean crystallization. Therefore, the various existing radiometric dating for 60025 sets the lunar magma ocean to have fully solidified by either 4.51 or 4.38 billion years ago, constraining the two respective lunar differentiation timescales to <30 (short-lived) or ~130–150 (long-lived) million years.

[1] Department of Earth and Planetary Sciences, Harvard University, Cambridge, MA 02138, USA. ✉email: hairuo.fu@g.harvard.edu

The Earth–Moon system has been hypothesized to originate from a giant impact early in the solar system history[1,2]. New and traditional theories debate whether the Moon-forming giant impact carried sufficiently high energy that vaporized the Mars-sized impactor (Theia) and proto-Earth to homogenize Earth–Moon chemical and isotopic compositions (e.g. ref. [3]), or whether it was less energetic and led to incomplete mixing of the impactors (e.g. refs. [1,2,4,5]), that can permit chemical and isotopic heterogeneities of the Earth–Moon system.

These hypotheses are testable with geochemical observations. For example, for mass-independent isotopic compositions, the high-energy giant impact scenario (Synestia)[3] predicts an Earth–Moon isotopic similarity [recently discovered for $\Delta^{17}O$[6], $\varepsilon^{50}Ti$[7], and $\varepsilon^{54}Cr$[8,9]] due to extensive isotope equilibration within the Moon-forming disk in a well-mixed silicate vapor. In contrast, the traditional giant-impact scenarios allow for considerable Earth–Moon isotopic differences considering the distinct mass-independent isotopic compositions of the impactors (Theia and the Proto-Earth), hinted by the documented isotopic variability among present Solar System objects[7,10]. For mass-dependent isotopic compositions of lithophile elements (e.g., $\delta^{26/24}Mg$, $\delta^{44/40}Ca$, $\delta^{56/54}Fe$), the differentiated impactors' mantle layers are expected to be isotopically fractionated caused by planetary magmatic differentiation. As a result, the complete isotopic mixing expected in the Synestia hypothesis still requires indistinguishable mass-dependent isotopic compositions of the bulk silicate Earth (BSE) and Moon (BSM)[3]. However, the traditional giant-impact models can give rise to marked mass-dependent isotopic differences between the BSE and BSM, considering that the BSM formed by sampling a minimal mass fraction (~2%) from the larger, isotopically heterogenous and insufficiently mixed impactors' silicate mantle.

Recent studies have shown consistent $\delta^{26/24}Mg$ and $\delta^{56/54}Fe$ values of the BSE and BSM, supporting an isotope equilibration of the Earth–Moon system before the terrestrial and lunar differentiation[11–15]. Attempts have been made to infer the mass-dependent Ca isotopic compositions ($\delta^{44/40}Ca$) of the BSM, suggested to be similar to the BSE[16]. However, reliable quantifications remain lacking due to an underrepresented sample pool of analysis (data from lunar meteorites only) and insufficient constraints provided by a preliminary binary mixing model[16]. The model treats the $\delta^{44/40}Ca$ values of the two mixing end-members (the lunar mantle and crust) as constants without associated uncertainties[16], which does not fully account for the complicated lunar isotopic heterogeneity and hence limits the reliability of the conclusions. Since Ca is one of the most refractory major elements, whose mass-dependent isotopic fractionation is not affected by planetary accretion, core formation, or magmatic degassing, the BSM and BSE $\delta^{44/40}Ca$ signatures preserve those of their building materials and give direct evidence for the Moon-forming mechanism. Therefore, the BSM $\delta^{44/40}Ca$ composition necessitates a more robust quantitative resolution to help clarify the origin of the primordial Earth–Moon system.

Following the Moon-forming giant impact and accretion, the lunar differentiation started with a hypothesized lunar magma ocean (LMO) of molten silicate rock, which continued to solidify as the Moon cooled[17,18]. $\delta^{26/24}Mg$ and $\delta^{56/54}Fe$ variations throughout the LMO crystallization have been observed and demonstrated as the result of lunar igneous processes[11,15]. In comparison, $\delta^{44/40}Ca$ evolution during the LMO crystallization awaits new critical investigations called for by recent testing of mineral-melt Ca-isotope fractionation factors, particularly for plagioclase[19]. Importantly, when multiple stable isotopic systematics are used in conjunction, they may yield higher confidence in the significance of each record and serve as key differentiation indexes to determine the evolution stage of LMO products. The magmatic context provided by stable isotopes can then be paired with the radiometric dating of lunar samples to constrain the relative and absolute timeline of the lunar differentiation.

To resolve the BSM $\delta^{44/40}Ca$ composition and trace the progression of the LMO crystallization, we performed high-precision Ca-isotope measurements for 13 lunar rocks and minerals (Supplementary Table 1) returned from the Apollo missions. These measurements include the first Ca-isotope analyses for lunar olivine and ferroan anorthosite (FAN) samples considered as primary floatation cumulates from the LMO.

Results and discussion

Ca-isotope composition of the Moon and implications for the Moon's high-energy giant-impact origin. Our $\delta^{44/40}Ca$ measurements (relative to standard SRM915a) for lunar basalts show consistency with recently reported values analyzed using a collision-cell MC-ICP-MS method[20] ($\delta^{44/40}Ca = \sim 0.8–0.9‰$) (Fig. 1a). In particular, our analyses for three lunar basalts (15555, 70215, 74275) yielded indistinguishable values (Supplementary Table 1) for the same ones measured by Klaver et al.[20], demonstrating the inter-lab reproducibility and accuracy of the analyses. Some earlier $\delta^{44/40}Ca$ measurements for the lunar basalts reported systematically heavier Ca-isotope compositions ($\delta^{44/40}Ca = \sim 0.9–1.0‰$)[21,22] or a larger spread ($\delta^{44/40}Ca = 0.76–1.10‰$) with large analytical uncertainties (>0.05‰ overall)[23], indicating an ongoing inter-lab difference that requires more efforts to address. Combining our lunar basalt measurements and data from Klaver et al.[20] yields distinct average $\delta^{44/40}Ca$ values for low-Ti basalts [$0.868 \pm 0.007‰$, two standard errors (2SEs)] and high-Ti basalts ($0.824 \pm 0.007‰$), a significant difference that traces mass-dependent isotopic fractionation during lunar igneous processes (Fig. 1a).

Our results for the three FAN samples and the plagioclase in 76535 (a lunar troctolite) exhibit lighter Ca-isotope compositions ($\delta^{44/40}Ca = \sim 0.7–0.8‰$, averaging at $0.756 \pm 0.036‰$) that agree with previously reported data for lunar meteorites (feldspathic breccias)[16,24] (Fig. 1), further affirming the overall lighter $\delta^{44/40}Ca$ value of the lunar highland. The average of these available values gives $\delta^{44/40}Ca = 0.763 \pm 0.012‰$ (Fig. 1a) for the mean of the lunar FANs and feldspathic breccias. In addition, the analyzed olivine mineral separate from 12012, a low-Ti basalt, is substantially heavier in Ca isotopes ($\delta^{44/40}Ca = 1.09 \pm 0.03‰$) (Fig. 1a). This result supports the heavy Ca-isotope enrichment of lunar olivine, which, furthermore, infers that the lighter Ca isotopes of lunar basalts and highlands are likely balanced by the heavier Ca isotopes in the lunar mantle, in line with some previous predictions[25].

The FANs are thought to be the primary floatation cumulates crystallizing from the late-stage LMO (~70–100%) (e.g. refs. [26,27]), making them valuable candidates to probe the initial isotopic compositions of the LMO. Some recent studies suggested that a part of the lunar anorthositic samples might trace chemical equilibration with a minor amount of KREEP [highly enriched in potassium (K), rare earth elements (REE), and phosphorus (P)] component (<1%) due to lunar partial mantle overturn[28,29]. Given the relatively low Ca content of the KREEP (~7 wt%)[30] compared to the Ca-rich lunar plagioclase (~19 wt%)[31], a maximum of 1% involvement of the KREEP would not modify the primary Ca isotopic signature of the plagioclase acquired from the initial LMO crystallization.

We developed a Monte Carlo method that uses two representative LMO crystallization models of experiments[26] and thermodynamic phase equilibrium[27] to solve for the best-fit initial $\delta^{44/40}Ca$ values of the LMO that reproduce the observed range of FANs and feldspathic breccias (Fig. 1b and c)

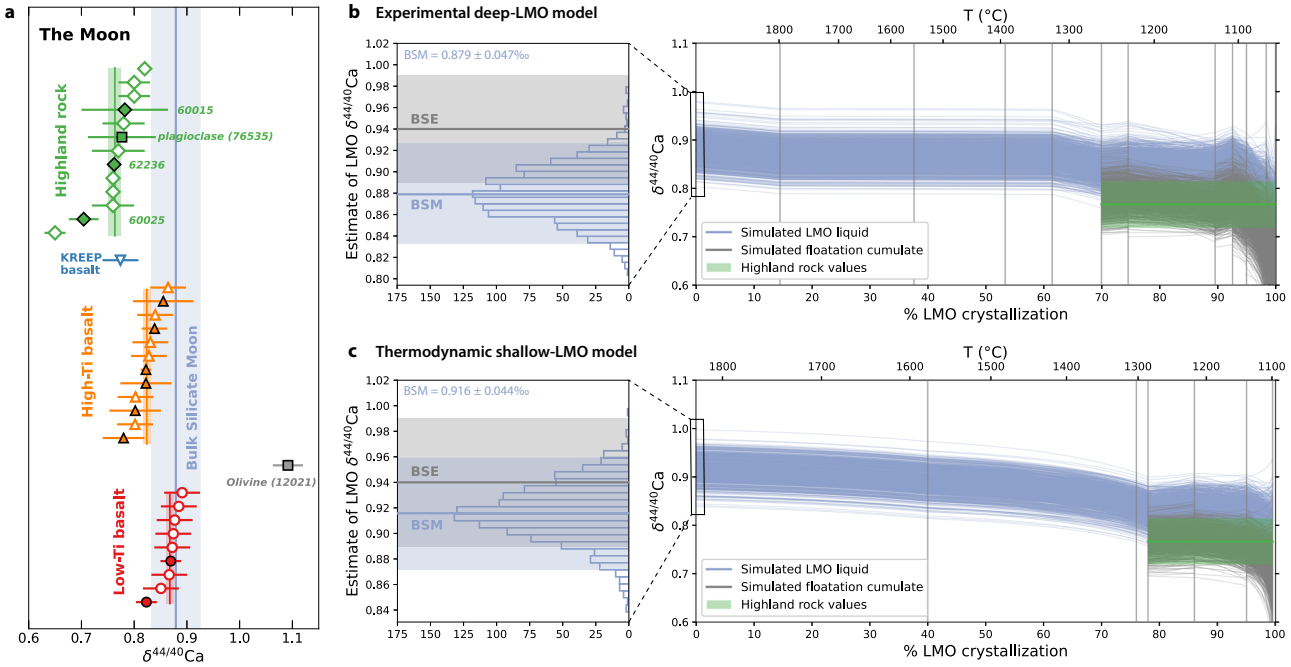

Fig. 1 Ca-isotope composition of the Moon. a $\delta^{44/40}$Ca values of lunar basalts, highland feldspathic rocks, minerals, and the estimated Bulk Silicate Moon (BSM). Closed/open symbols show data analyzed in this study/reported from the literature [lunar basalts from ref. [20], highland feldspathic meteorites (open diamonds) from refs. [16,24]]. The colored horizontal lines and shaded bands represent the means and two standard errors (2SE) of individual groups. The presented BSM values (0.879 ± 0.047‰) (95% confidence intervals) are the results of the inversion of the LMO using the preferred experimental deep-LMO model[26] (Fig. 1b). See Supplementary Table 1 for details of data. **b** and **c** Monte Carlo simulations to back-calculate the BSM values with the deep[26] and shallow[27] LMO models (Supplementary Note 1). The enclosed initial $\delta^{44/40}$Ca values (at 0% LMO crystallization), tied with individual $\delta^{44/40}$Ca evolution curves of the LMO (purple line), define the plausible range of BSM $\delta^{44/40}$Ca that could reproduce the floatation cumulates (grey line) consistent with observations. The green line and band show the mean and two standard deviations of the highland rocks. The vertical grey lines delineate the individual crystallization stages of each model. The histograms display the estimated BSM values obtained from the two models, where the horizontal lines and bands plot the mean $\delta^{44/40}$Ca values and 2SEs of the BSM (this study) and BSE[34].

(Supplementary Note 1). These two LMO crystallization models also account for the debated initial LMO depth, hypothesized to range from as shallow as 500 km[27,28,32] to as deep as the whole Moon (e.g. refs. [26,29,33]). The experimental model[26] assumes a deep (~1150 km), nearly whole-Moon, LMO crystallization condition, and the thermodynamic model[27] assumes an initial ~500 km shallow LMO. Despite the different assumptions on the LMO depth, both models involve similar fractionating mineral phases, including olivine, orthopyroxene, clinopyroxene, and plagioclase, but with moderately different mass proportions and fractionating orders (Supplementary Tables 2 and 3). To account for the temperature dependence of isotopic fractionation factors, our isotopic models use experimentally determined crystallization temperature sequences obtained for deep[26] and shallow[27] LMO crystallization scenarios.

The estimated LMO initial $\delta^{44/40}$Ca values have a mean of 0.879 ± 0.047‰ (95% confidence intervals) using the experimental deep-LMO mineralogy sequence[26] and 0.916 ± 0.044‰ using the thermodynamic shallow-LMO model[27], both overlapping within error with the estimated BSE value of 0.94 ± 0.05‰[34] (Fig. 1b and c) (Supplementary Note 1). *T*-tests for both LMO estimates find that the null hypothesis of the LMO and BSE having the same $\delta^{44/40}$Ca cannot be rejected at a significance level of 0.05 (*t*-statistic = 1.78 and 0.72, both <1.96). Recently, more geophysical and geochemical evidence has been uncovered that suggests a high-temperature origin of the Moon and an initially fully molten Moon. These inferences come from the simulation of the Moon-forming impact and the Moon's accretion (>3000–4000 K)[3,5], metal-silicate partitioning experiments (>2600–3700 K)[35], and the depletion pattern of lunar and terrestrial moderately volatile elements[3,36]. Therefore, we take the initial LMO $\delta^{44/40}$Ca = 0.879 ± 0.047‰ obtained from the experimental 1150 km-deep LMO model[26], whose depth also agrees with evidence from mass-balance calculations of Nd, Sr, and Hf isotopes[33]. As such, the LMO $\delta^{44/40}$Ca composition (0.879 ± 0.047‰) is equivalent to that of the BSM.

The mass-dependent stable isotopic closeness between the BSM and BSE has also been discovered for $\delta^{26/24}$Mg and $\delta^{56/54}$Fe[11–15]. These indistinguishable mass-dependent isotopic ratios of the BSM and BSE lend strong support to a high-energy giant-impact condition (Synestia) that adequately homogenized isotopic compositions within the Moon-forming disk[3]. In comparison, the traditional, lower-energy, giant-impact scenarios[1,2,4,5] would predict notable mass-dependent stable isotopic heterogeneities of the Earth–Moon system. This is because in these less energetic impact scenarios, the silicate Moon forms by sampling a minimal mass fraction (~2%) from the incomplete mixture of the massive, isotopically fractionated mantle layers of the impactors (Theia and the Proto-Earth). Due to the inadequate mixing of the impactors' mantle, this extracted minor silicate fraction (the BSM) would be difficult to average out the stable isotopic variability inherited from the impactors' mantle and, thereby, is likely isotopically distinct from the bulk silicate mixture (later becoming the BSE).

Especially, under traditional giant-impact hypotheses, regardless of how much of the Moon's building materials were derived from Theia or the proto-Earth [a classic question approached extensively with mass-independent isotopic anomalies (e.g. refs. [6,7])], the BSM would nevertheless likely sample and reflect the impactors' preexisting mass-dependent isotopic heterogeneities because the

BSM accretes from such small proportions of either impactor's mantle. Therefore, the BSM and BSE having the same mass-dependent stable isotopic signatures is a low-probability outcome of the traditional giant-impact models, irrespective of (i) whether the Moon's materials are sourced primarily from Theia or the proto-Earth or (ii) the two impactors shared identical pre-impact bulk mass-dependent isotopic compositions. We conclude that the observed BSM-BSE similarity in mass-dependent stable isotopes ($\delta^{26/24}$Mg, $\delta^{26/24}$Ca, and $\delta^{56/54}$Fe) is consistent with the Earth-Moon high-energy giant-impact origin[3] and not readily explained by the traditional Moon-forming giant-impact models.

Tracing the lunar differentiation with Ca and Mg isotopes. Once we obtain the initial stable isotopic compositions of the LMO, we can model the stable isotopic fractionation during the LMO crystallization and compare the results with lunar samples to understand the evolution of the lunar differentiation. For this purpose, we forward modeled the Ca and Mg isotopic fractionation throughout the LMO solidification (Supplementary Note 3), whose temperature-dependent mineral-melt fractionation factors have been better constrained in recent years[11,19,37,38] (Supplementary Note 2). The isotopic evolution was calculated with both cumulate mineral sequences established by the deep-LMO experiments[26] and shallow-LMO thermodynamic modeling[27] to test the influence of assumed LMO depths (Fig. 2).

Figure 2a and d illustrate the $\delta^{44/40}$Ca and $\delta^{26/24}$Mg variations of the LMO liquid, sinking mantle cumulates (such as olivine, pyroxene, spinel, and ilmenite), and floatation cumulates (plagioclase), which behave overall similarly for the two models. For both models, $\delta^{44/40}$Ca and $\delta^{26/24}$Mg exhibit remarkable fractionation in the LMO liquid and cumulate (~0.2‰ to ~0.9‰) during the late-stage evolution (>70% crystallization) (Fig. 2a and d), enabling the two systematics to estimate the evolution stage of lunar samples. Note that the LMO crystallization models predict an overall decrease in $\delta^{44/40}$Ca during the late-stage magmatic differentiation (>70%) (Fig. 2a and d), in contrast to the typical terrestrial magma systems that produce increasing $\delta^{44/40}$Ca in the late, felsic crystallization stage[19, 39]. This contrasting behavior is because feldspar (preferentially taking lighter Ca isotopes) is typically the major Ca host of the fractionating phases in the evolved terrestrial magma, while the abundant pigeonite or low-Ca augite (preferentially taking heavier Ca isotopes) chiefly control the late-stage LMO isotopic fractionation and render the residual LMO liquid overall lighter in Ca isotopes.

In Fig. 2b and e, we present the cross-plots of $\delta^{44/40}$Ca versus $\delta^{26/24}$Mg for the modeled LMO isotopic variations as a function of LMO crystallization. Ca and Mg isotope data for mare basalts from this study and the literature[11,20], for which $\delta^{44/40}$Ca and $\delta^{26/24}$Mg have been both analyzed, are also shown. Low-degree partial melting of lunar mantle cumulates has been suggested as the origin of mare basalts[11,20]. At low degrees of partial melting, the isotopic fractionation effect caused by (i) the crystallization of cumulates out of the LMO and (ii) the subsequent cumulates' partial melting that produced mare basalts should counteract and nearly cancel out each other[11]. Therefore, the cumulate partial melting hypothesis for the mare basalt petrogenesis would predict the mare basalts' isotopic compositions approximating the instantaneous LMO compositions from which their mantle sources formed. Consistently for both LMO models, the $\delta^{44/40}$Ca and $\delta^{26/24}$Mg data of the mare basalts fall closely along the modeled LMO liquid line of descent (Fig. 2b and e) in evolved stages (from ~75% to 98% crystallization). The excellent correspondence between the multi-stable-isotope data and the LMO isotopic fractionation model strongly supports the mare basalts formation by partially melting lunar mantle cumulates and constrains these cumulates to have precipitated late in the LMO magmatic differentiation[11,20].

Next, we compared the isotopic signatures of lunar feldspathic samples with modeled floatation cumulates to probe their magmatic context (Fig. 2c and f). For both LMO crystallization scenarios, the Ca and Mg isotopic data of the two FAN samples, 60015 and 60025, agree well with the predicted values for primary flotation crusts and indicate a formation near the end of LMO differentiation (>99% solidification). 62236 is not directly comparable with the modeled flotation cumulates because mafic minerals, rather than plagioclase, are the main host of Mg[11]. The plagioclase composition of 76535, a troctolite sample from the Mg-suite, falls between ~75% and 95% of LMO crystallization considering uncertainties, reflecting a relatively less-evolved plagioclase component compared to those in the FAN samples (Fig. 2c and f). Some existing Sm–Nd geochronologic constraints suggest that 76535 might have formed later than 60025[40]. This apparent discrepancy that an earlier-stage mineral composition preserved in a later-forming troctolite could be reconciled by 76535 forming as deep cumulates produced by lunar mantle overturns that postdate the LMO crystallization. Such petrogenic processes may have involved either/both (i) mineral precipitation from the partial melts produced by overturned earlier mafic cumulates or/and (ii) hybrid partial melting of the earlier mafic cumulates and later floatation cumulates[40]. Considering this possibility, only the analyzed FAN samples (60015 and 60025) are taken as credible indicators of the degree of LMO differentiation associated with their formation ages, which are independently defined by available radiometric dating.

While the crystallization age of 60015 remains largely unclear, extensive geochronologic investigations have been performed for 60025 to understand the significance of its age for the Moon's formation and differentiation. Temporally, 60025 has been variably associated with the formation of (i) young lunar crusts during a rapid LMO crystallization[41,42] and (ii) early lunar crusts during a prolonged crustal formation and LMO crystallization[43]. These competing interpretations stem from two principal sources. First, the discrepant and controversial absolute dates that were obtained using various chronometers[41,44]. Second, the propagated uncertainties when relating these debated dates with those for other lunar differentiation events to establish relative temporal relationships (such as the formation of KREEP and source regions of lunar basalts)[41–43]. In circumventing the ambiguities led by traditional methodologies that use comparison between debated absolute ages, our stable isotopic evidence provides an independent and critical resolution elucidating that 60025 marks the final solidification of the LMO. As a further profound implication, the formation age of 60025 should be used unambiguously to indicate the termination of the lunar differentiation.

Timeline of the Moon's formation and differentiation. The resolved lunar differentiation context of 60025 warrants a new calibration of the early lunar chronology. To gain new insights into the lunar differentiation timeline, we synthesized a database of representative chronologic evidence for various evolution stages of the LMO solidification (Fig. 3). The Moon's formation (whose age approximates the moon-forming giant impact and initial crystallization of the Moon) has been constrained to from ~30 to 60 million years (Myr) after the formation of the solar system by ^{182}Hf–^{182}W systematics for the silicate Moon[45–47], lunar metals[48] and Earth's mantle[49] and Lu–Hf model ages for lunar zircons[50]. Early lunar differentiation (<50% LMO crystallization) may be best represented by a dunite sample, 72415, the possibly oldest lunar rock sampled from early mantle cumulates [4527 ± 92 million years ago (Ma)][51]. Based on its nearly identical

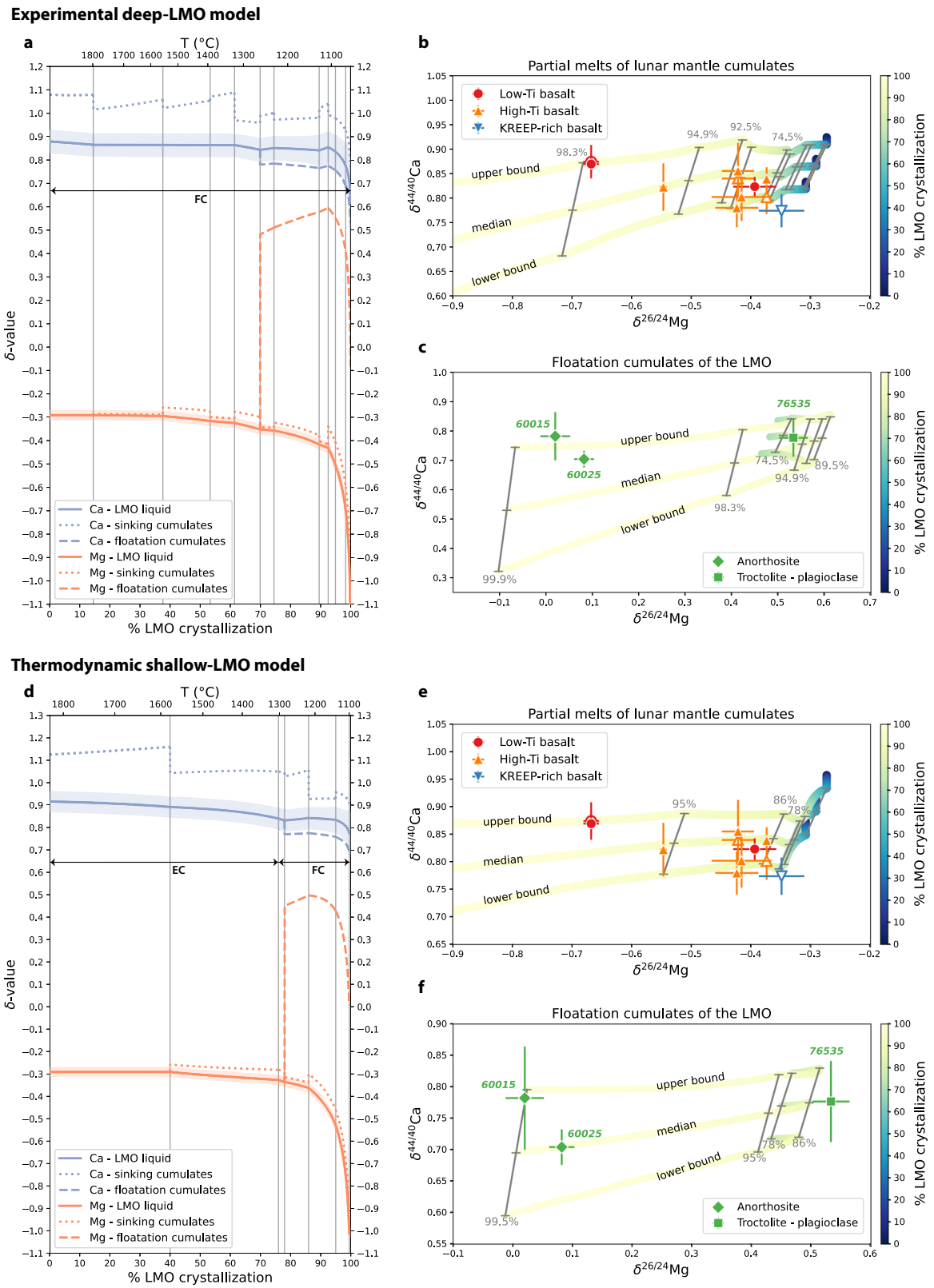

Mg isotope signature to the BSM[11], it likely reflects early LMO solidification before plagioclase started to saturate and prominently fractionate Mg isotopes (we assign it with a nominal 40% of LMO solidification between 0% and 80%) (Fig. 3).

Late-stage lunar differentiation is delineated by the formation of the lunar crust and KREEP sources. These dates include (i) an average ^{147}Sm–^{143}Nd isochron age (4456 ± 40 Ma) quantified by the mafic fractions from four anorthosites thought to reflect the crystallization of early lunar crust[52] (>75% LMO solidification); (ii) ^{147}Sm–^{143}Nd and ^{176}Lu–^{177}Hf model ages for the source of KREEP basalts (4368 ± 29 Ma)[42] and the oldest lunar zircons (4417 ± 6 Ma)[53] considered crystallizing from KREEP-rich magma (>95% LMO solidification); and (iii) distinguished Pb–Pb isochron ages for plagioclase (4510 ± 10 Ma)[44] and pyroxene

Fig. 2 Ca and Mg isotopic evolution of the LMO. a Modeling $\delta^{44/40}$Ca and $\delta^{26/24}$Mg variations throughout the LMO crystallization using a mineral sequence established by experiments assuming a deep-LMO (~1150 km)[26]. The LMO liquid, sinking cumulates, and flotation cumulates are shown by solid, dotted, and dashed lines, respectively. The model takes a Monte Carlo method that accounts for propagated errors in the BSM composition (initial LMO value) and temperature-dependent fractionation factors (Supplementary Note 3). The lines and envelopes show the means and associated 95% confidence intervals. EC equilibrium crystallization, FC fractional crystallization. **b** and **c** Cross-plot of $\delta^{44/40}$Ca and $\delta^{26/24}$Mg showing the comparison between isotopic data and modeling. Mg isotope data are from the literature;[11] Ca isotope data are from this study (closed symbols) and the literature[20] (open symbols). All error bars on the data are 2SEs. For the modeling curves, **b** plots the modeled LMO liquid line of descent, and **c** plots the modeled floatation cumulates. The median and upper- and lower-bound curves reflect the mean and 95% confidence bounds as shown in (**a**). The percent of LMO crystallization of the modeling curves is color-coded (color bars on the right), with each crystallization stage signified by the grey line segment and adjacent label (i.e., 78%, 86%, and 95%). **d**–**f** show the modeled results using a thermodynamic shallow-LMO (500 km) mineral sequence[27].

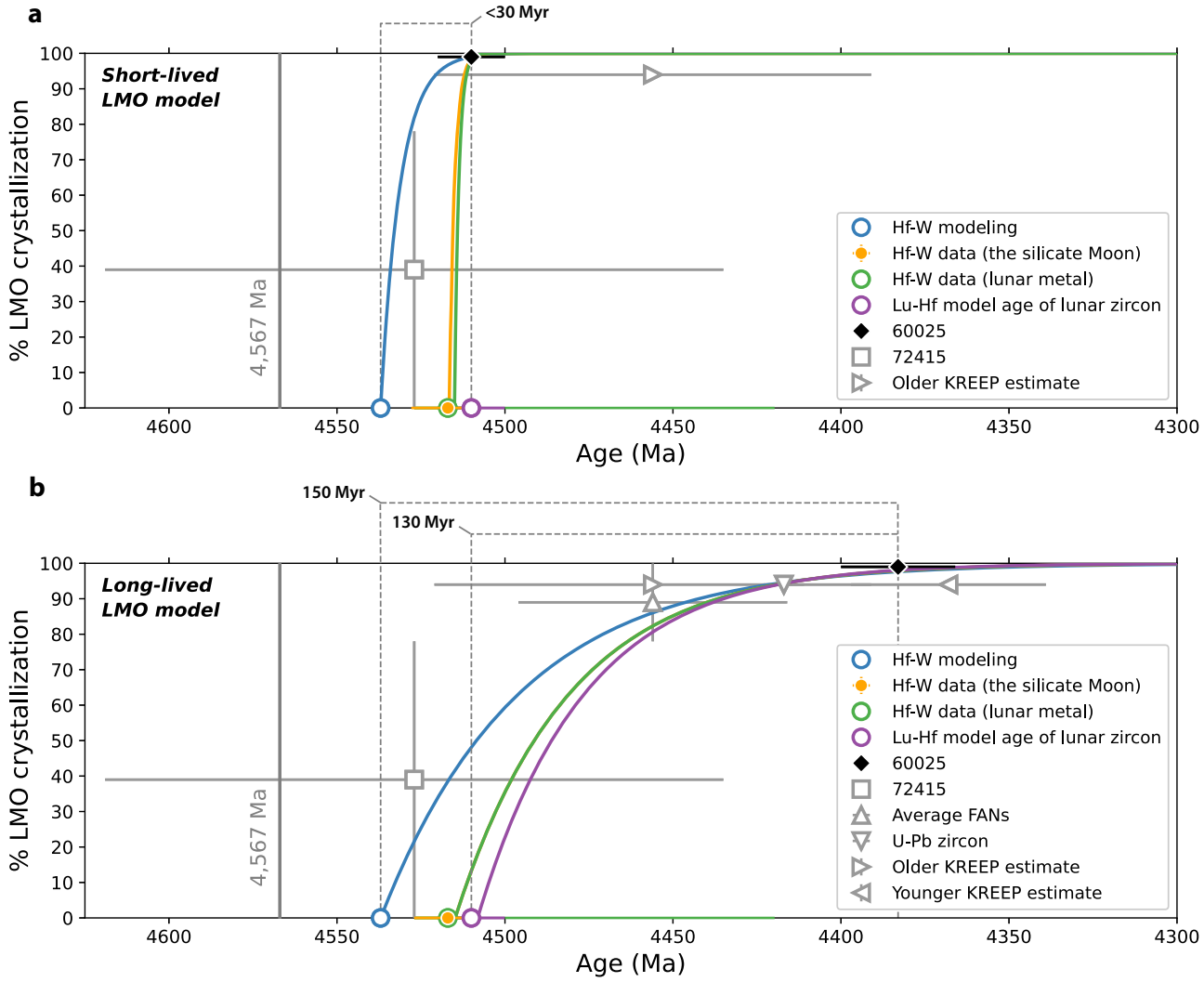

Fig. 3 Two lunar differentiation models permitted by chronologic evidence. a A short-lived LMO crystallization (<30 Myr) required by the old formation age of 60025 (4510 ± 10 Ma)[44]. **b** A long-lived LMO crystallization (~130–150 Myr) necessitated by the proposed young age of 60025 (4383 ± 17 Ma)[40]. Error bars on the data points represent two standard errors. The solid vertical line indicates the formation age of the solar system corresponding to the age of calcium–aluminum-rich inclusions (CAIs)[60]. The curves illustrate exponential fittings to the data, whose color signifies which formation age of the Moon (the colored open circles) is used for the fitting. See text and Supplementary Tables 7 and 8 for the chronologic data and references.

(4359.2 ± 2.4 Ma)[41] and Sm–Nd ages for whole rock and mineral (4367 ± 11 Ma and 4319 ± 30/38 Ma)[41] for 60025 (>99% LMO solidification) (Fig. 3).

Given the distinct dates proposed for 60025, the age of 60025 plays an essential role in gauging the timespan of the lunar differentiation. We reexamined the previously reported Pb–Pb data from different labs[41, 44,54] and identified two well-defined while distinct mineral isochrons for 60025. One is for pyroxene (4359.2 ± 2.4 Ma, $n = 4$), which was originally explored by Borg et al.[41]. The other one is for plagioclase that yields an older age (4477.8 ± 35.7 Ma, $n = 6$) (Supplementary Fig. 5), overlapping within error with the 4510 ± 10 Ma plagioclase age obtained by[44]. The two mineral isochrons both intersect with the lunar ^{207}Pb/^{206}Pb–^{204}Pb/^{206}Pb growth curve, indicating products of a

multi-stage evolution (Supplementary Fig. 5). The presence of two credible and disparate isochron ages underscores the ongoing challenge of affirming 60025's formation age and emphasizes the various age possibilities of 60025.

We now discuss the plausible lunar differentiation scenarios permitted by the absolute dating for 60025. If the old 4510 ± 10 Ma Pb–Pb age[44] for pristine plagioclases in 60025 represents the sample's formation age, it requires an old Moon's formation predating ca. 4510 Ma and a rapid LMO solidification within the subsequent about <30 Myr (short-lived LMO model, Fig. 3a). Such a comparatively short duration has been explained by the LMO solidifying under a relatively high-conductivity anorthosite lid[55]. This scenario also agrees with the closeness of the mean age of dunite 72417 (4527 Ma)[51] and the Pb–Pb plagioclase age of 60025 (4510 Ma). Moreover, this model could reconcile with some of the older KREEP model age estimates averaging at 4456 ± 65 Ma[41] but would argue against the younger estimates [such as 4368 ± 29 Ma by Gaffney and Borg[42] and ca. 4270–4190 Ma by Maurice et al.[43]]. The 4510 ± 10 Ma age of 60025 thereby places an upper bound on the completion of the lunar differentiation.

If the young Pb–Pb isochron age for pyroxene and Sm–Nd isochron ages for 60025 are valid [averaging at 4383 ± 17 Ma at the solidus temperature of 60025[56]], this would suggest a prolonged lunar differentiation that lasted ~130–150 Myr based on the variously estimated timing of the giant impact (long-lived LMO model) (Fig. 3b). A slushy LMO, lacking efficient crystal-liquid separation, has been used to argue for this long timescale[57]. Moreover, the implied upper limit of ~150 Myr does not conflict with the modeled protracted LMO solidification taking up to ~200 Myr[43] involving mantle heat-piping and an anorthosite crust with a lower thermal conductivity than that of Elkins-Tanton et al.[55]. However, our results would necessitate the LMO solidification to complete by ca. 4387 Ma, disputing the models placing the end of the lunar differentiation between ca. 4270 and 4190 Ma[43]. Furthermore, differing from some prior suggestions that favor the younger (4368 ± 29 Ma) and preclude the older (4456 ± 65 Ma) KREEP model ages (e.g. ref. [41]), we find the young age of 60025 (4383 ± 17 Ma) compatible with both the proposed KREEP ages because 60025 likely documents the last solids of the LMO. Using these compatible age sets, we performed weighted-least-squares exponential fittings (Fig. 3b), which agree with an initial rapid crystallization of the LMO followed by slower cooling and prolonged solidification once the anorthosite crust formed[43,55,57]. In this model, the 4383 ± 17 Ma age of 60025 puts a lower bound on the cessation of the LMO crystallization.

Accounting for both the proposed old and young formation ages of 60025, our new isotopic evidence requires the LMO to have fully crystallized by either 4510 or 4387 Ma, with the total solidification timescales from <30 to ~130–150 Myr, respectively. A clearer distinction between a short-lived and long-lived LMO calls for better absolute chronology on the early LMO products to pair with stable isotopic constraints. We also conclude that the important magmatic differentiation context provided by the novel tool of multi-stable isotope systematics warrants more extensive applications in planetary problems in combination with traditional major and trace element methods.

Methods

Sample preparation and description. All sample preparations were performed in a clean room at Harvard University. About 10–100 mg (whole rocks) and 2–10 mg (separated minerals) of well-mixed powdered samples were dissolved in a mixture of HF–HCl–HNO_3. A CEM MARS 6 microwave digestion system and MARS Xpress high-pressure reaction vessels with a three-step procedure were used for sample dissolution; first step: 0.5 ml HF + 2 ml HNO_3 + 1 ml HCl; second step: 0.5 ml HNO_3 + 1.5 ml HCl + 1 ml H_2O; third step: 3–4 ml HNO_3; Power 400 W; Temperature 200 °C; 15 min ramping + 45 min holding + 30 min cooling. Dissolved samples from each step were dried with heat lamps in ultrapure N_2 and dissolved in adequate amounts of 2.5 N HCl after the third step to form a 10 µg/µl Ca solution. To correct the isotopic fractionation produced by chemical separation and instrumental analysis, a double spike technique was used by adding a certain amount of ^{43}Ca–^{48}Ca double spike solution to each sample solution before column chemistry[58]. Calcium was purified by ion-exchange chromatography using a cation exchange resin (Bio-Rad AG50W-X12 [200–400 mesh]) in 2.5 N HCl media following a previously established procedure[58]. Each sample was processed through the column chemistry twice to ensure that the final Ca solution was free of other elements. About 5.0 µg Ca from the purified solution was loaded as $Ca(NO_3)_2$ onto one of the side filaments of a zone-refined Re triple filament assembly[58].

The set of lunar samples analyzed for Ca isotopes in this study is the same as in Sedaghatpour and Jacobsen[11] for Mg isotopic analysis, from which detailed descriptions of the samples are provided (Supplementary Information: Lunar samples description).

Ca-isotope measurement. Calcium isotopic ratios were measured using a GV Isoprobe-T thermal ionization mass spectrometry (TIMS) at Harvard University. All Ca isotopes were measured in a two-sequence method reported earlier by our group[35]. In the first sequence, the peaks for ^{40}Ca to ^{44}Ca were collected. In this step,^{41}K was also measured to monitor possible isobaric interference of ^{40}K. Furthermore, a mass range from 39 to 49 was scanned to ensure there were no ^{47}Ti, ^{49}Ti, or double-charged Sr species ($^{84}Sr^{2+}$ and $^{88}Sr^{2+}$) to interfere with Ca isotope measurements. Each analysis includes 20 blocks, 10 cycles each with a 6-s integration time for each sequence, followed by a 1-s waiting time, resulting in a total analytical time of ~120 min (including the 25-min heating routine). Isotope data are reported as part per thousand deviations from spiked measurements of NIST SRM915a standard with δ-notation (Supplementary Table 1):

$$\delta^{44/i}\mathrm{Ca}(‰) = [(^{44}\mathrm{Ca}/^{i}\mathrm{Ca})_{\mathrm{sample}}/(^{44}\mathrm{Ca}/^{i}\mathrm{Ca})_{\mathrm{SRM915a}} - 1]\times 1000 \quad (1)$$

where i is the Ca isotope mass 40 or 42. Sample analysis was done multiple times for each sample, with the averages and external reproducibility (two standard errors, 2SE) of $\delta^{44/40}Ca$ and $\delta^{44/42}Ca$ reported in Supplementary Table 1. Combined spiked and unspiked measurements of NIST SRM915a yield $^{40}Ca/^{44}Ca = 47.1562$ and $^{42}Ca/^{44}Ca = 0.3121794$, which are used to calculate the δ-values. Standards measured relative to these values are BHVO-2 with $\delta^{44/40}Ca = 0.85 \pm 0.03‰$ and IAPSO seawater with $\delta^{44/40}Ca = 1.83 \pm 0.03‰$.

In Supplementary Fig. 1, we plot all measured lunar samples in a three-Ca-isotope diagram of $^{44}Ca/^{42}Ca$ versus $^{44}Ca/^{40}Ca$. Most data plot closely along the expected lines of mass-dependent relationships[44] within uncertainty (Supplementary Table 1). To more firmly ascertain the $\delta^{44/40}Ca$ values of the samples, we also calculate $\delta^{44/40}Ca$ from the measured $\delta^{44/42}Ca$ according to mass-dependent relationships ($\delta^{44/40}Ca \approx 2.0483*\delta^{44/42}Ca$)[59]. These calculated $\delta^{44/40}Ca$ values from $\delta^{44/42}Ca$ were then weight-averaged with the directly measured $\delta^{44/40}Ca$ to obtain the mean $\delta^{44/40}Ca$ values and propagated uncertainties (Supplementary Table 1), taken as the best estimate in this study.

Data availability

All Ca isotope data for the analyzed lunar samples of this study are available on Zenodo (https://doi.org/10.5281/zenodo.8197851).

Code availability

Python codes for determining the LMO initial Ca isotope composition and modeling the Ca and Mg isotopic fractionation during the LMO crystallization can be found on Zenodo (https://doi.org/10.5281/zenodo.8197851).

Received: 9 March 2023; Accepted: 24 August 2023;
Published online: 05 September 2023

References

1. Canup, R. M. & Asphaug, E. Origin of the Moon in a giant impact near the end of the Earth's formation. *Nature* **412**, 708–712 (2001).
2. Canup, R. M. Simulations of a late lunar-forming impact. *Icarus* **168**, 433–456 (2004).
3. Lock, S. J. et al. The origin of the Moon within a terrestrial synestia. *J. Geophys. Res.: Planets* **123**, 910–951 (2018).
4. Canup, R. M. Accretion of the Earth. *Philos. Trans. R. Soc. A* **366**, 4061–4075 (2008).
5. Canup, R. M., Visscher, C., Salmon, J. & Fegley, B. Lunar volatile depletion due to incomplete accretion within an impact-generated disk. *Nat. Geosci.* **8**, 918–921 (2015).
6. Young, E. D. et al. Oxygen isotopic evidence for vigorous mixing during the Moon-forming giant impact. *Science* **351**, 493–496 (2016).
7. Zhang, J., Dauphas, N., Davis, A. M., Leya, I. & Fedkin, A. V. The proto-Earth as a significant source of lunar material. *Nat. Geosci.* **5**, 251–255 (2012).
8. Qin, L., Alexander, C. M., Carlson, R. W., Horan, M. F. & Yokoyama, T. Contributors to chromium isotope variation of meteorites. *Geochim. Cosmochim. Acta* **74**, 1122–1145 (2010).
9. Mougel, B., Moynier, F. & Gopel, C. Chromium isotopic homogeneity between the Moon, the Earth, and enstatite chondrites. *Earth Planet. Sci. Lett.* **481**, 1–8 (2018).
10. Ireland, T. R., Avila, J., Greenwood, R. C., Hicks, L. J. & Bridges, J. C. Oxygen isotopes and sampling of the solar system. *Space Sci. Rev.* **216**, 1–60 (2020).
11. Sedaghatpour, F. & Jacobsen, S. B. Magnesium stable isotopes support the lunar magma ocean cumulate remelting model for mare basalts. *Proc. Natl. Acad. Sci. USA* **116**, 73–78 (2019).
12. Sedaghatpour, F., Teng, F., Liu, Y., Sears, D. W. & Taylor, L. A. Magnesium isotopic composition of the Moon. *Geochim. Cosmochim. Acta* **120**, 1–16 (2013).
13. Poitrasson, F., Zambardi, T., Magna, T. & Neal, C. R. A reassessment of the iron isotope composition of the Moon and its implications for the accretion and differentiation of terrestrial planets. *Geochim. Cosmochim. Acta* **267**, 257–274 (2019).
14. Sossi, P. A. & Moynier, F. Chemical and isotopic kinship of iron in the Earth and Moon deduced from the lunar Mg-Suite. *Earth Planet. Sci. Lett.* **471**, 125–135 (2017).
15. Wang, K., Jacobsen, S. B., Sedaghatpour, F., Chen, H. & Korotev, R. L. The earliest lunar magma ocean differentiation recorded in Fe isotopes. *Earth Planet. Sci. Lett.* **430**, 202–208 (2015).
16. Wu, W., Xu, Y.-G., Zhang, Z.-F. & Li, X. Calcium isotopic composition of the lunar crust, mantle, and bulk silicate Moon: a preliminary study. *Geochim. Cosmochim. Acta* **270**, 313–324 (2020).
17. Smith, J. et al. Petrologic history of the moon inferred from petrography, mineralogy, and petrogenesis of Apollo 11 rocks. In *Proc. Apollo 11 Lunar Science Conference* (ed Levinson, A. A.) Vol. 1, 897–925 (Pergamon Press, New York, 1970).
18. Wood, J. A., Dickey, J. S., Marvin, U. B. & Powell, B. N. Lunar anorthosites. *Science* **167**, 602–604 (1970).
19. Fu, H., Jacobsen, S. B., Larsen, B. T. & Eriksen, Z. Ca-isotopes as a robust tracer of magmatic differentiation. *Earth Planet. Sci. Lett.* **594**, 117743 (2022).
20. Klaver, M. et al. The Ca isotope composition of mare basalts as a probe into the heterogeneous lunar mantle. *Earth Planet. Sci. Lett.* **570**, 117079 (2021).
21. Simon, J. I. & DePaolo, D. J. Stable calcium isotopic composition of meteorites and rocky planets. *Earth Planet. Sci. Lett.* **289**, 457–466 (2010).
22. Simon, J. I. et al. Calcium and titanium isotope fractionation in refractory inclusions: tracers of condensation and inheritance in the early solar protoplanetary disk. *Earth Planet. Sci. Lett.* **472**, 277–288 (2017).
23. Valdes, M. C., Moreira, M. A., Foriel, J. & Moynier, F. The nature of Earth's building blocks as revealed by calcium isotopes. *Earth Planet. Sci. Lett.* **394**, 135–145 (2014).
24. Schiller, M., Bizzarro, M. & Fernandes, V. A. Isotopic evolution of the protoplanetary disk and the building blocks of Earth and the Moon. *Nature* **555**, 507–510 (2018).
25. Huang, F., Zhou, C., Wang, W., Kang, J. & Wu, Z. First-principles calculations of equilibrium Ca isotope fractionation: implications for oldhamite formation and evolution of lunar magma ocean. *Earth Planet. Sci. Lett.* **510**, 153–160 (2019).
26. M. W. Schmidt, G. Kraettli, Experimental crystallization of the lunar magma ocean, initial selenotherm and density stratification, and implications for crust formation, overturn and the bulk silicate Moon composition. *J. Geophys. Res.: Planets* **127**, e2022JE007187 (2022).
27. Snyder, G. A., Taylor, A. & Neal, C. R. A chemical model for generating the sources of mare basalts: Combined equilibrium and fractional crystallization of the lunar magmasphere. *Geochim. Cosmochim. Acta* **56**, 3809–3823 (1992).
28. Ji, D. & Dygert, N. Trace element evidence for serial processing of the lunar flotation crust and a depleted bulk Moon. *Earth Planet. Sci. Lett.* **602**, 117958 (2023).
29. Pernet-Fisher, J. F., Deloule, E. & Joy, K. H. Evidence of chemical heterogeneity within lunar anorthosite parental magmas. *Geochim. Cosmochim. Acta* **266**, 109–130 (2019).
30. P. H. Warren, KREEP: major-element diversity, trace-element uniformity (almost). In: *Workshop on Moon in Transition: Apollo 14, KREEP, and Evolved Lunar Rocks* 149–153 (eds., Taylor, G. J. & Warren, P. H.) (Lunar and Planetary Institute, Houston, TX, 1989).
31. Papike, J., Taylor, L. & Simon, S. *Lunar Sourcebook, A User's Guide to Moon* Vol. 121 (Cambridge University Press, Cambridge, 1991).
32. Charlier, B., Grove, T. L., Namur, O. & Holtz, F. Crystallization of the lunar magma ocean and the primordial mantle-crust differentiation of the Moon. *Geochim. Cosmochim. Acta* **234**, 50–69 (2018).
33. Ranen, M. C. & Jacobsen, S. B. A deep lunar magma ocean based on neodymium, strontium and hafnium isotope mass balance. In *Proc.* 35th *Lunar Science Conference* (eds Stephen, M. & Eileen, S.) (2004).
34. Kang, J.-T. et al. Calcium isotopic fractionation in mantle peridotites by melting and metasomatism and Ca isotope composition of the Bulk Silicate Earth. *Earth Planet. Sci. Lett.* **474**, 128–137 (2017).
35. Steenstra, E. S., Berndt, J., Klemme, S., Fei, Y. & Westrenen, W. V. A possible high-temperature origin of the Moon and its geochemical consequences. *Earth Planet. Sci. Lett.* **538**, 116222 (2020).
36. Solomatova, N. V. & Caracas, R. Earth's volatile depletion trend is consistent with a high-energy Moon-forming impact of the Moon. *Commun. Earth Environ.* **4**, 38 (2023).
37. Schauble, E. A. First-principles estimates of equilibrium magnesium isotope fractionation in silicate, oxide, carbonate and hexaaquamagnesium(2+) crystals. *Geochim. Cosmochim. Acta* **75**, 844–869 (2011).
38. Gao, C. et al. Theoretical calculation of equilibrium Mg isotope fractionations between minerals and aqueous solutions. *Chem. Geol.* **488**, 62–75 (2018).
39. Zhu, H. et al. Calcium isotopic fractionation during magma differentiation: constraints from volcanic glasses from the eastern Manus Basin. *Geochim. Cosmochim. Acta* **305**, 228–242 (2021).
40. Nelson, W. S., Hammer, J. E., Shea, T., Hellebrand, E. & Jeffrey, T. G. Chemical heterogeneities reveal early rapid cooling of Apollo Troctolite 76535. *Nat. Commun.* **12**, 7054 (2021).
41. Borg, L. E., Connelly, J. N., Boyet, M. & Carlson, R. W. Chronological evidence that the Moon is either young or did not have a global magma ocean. *Nature* **477**, 70–72 (2011).
42. Gaffney, A. M. & Borg, L. E. A young solidification age for the lunar magma ocean. *Geochim. Cosmochim. Acta* **140**, 227–240 (2014).
43. Maurice, M., Tosi, N., Schwinger, S., Breuer, D. & Kleine, T. A long-lived magma ocean on a young Moon. *Sci. Adv.* **6**, eaba8949 (2020).
44. Hanan, B. B. & Tilton, G. R. 60025: relict of primitive lunar crust? *Earth Planet. Sci. Lett.* **84**, 15–21 (1987).
45. Thiemens, M. M., Sprung, P., Fonseca, R. O., Leitzke, F. P. & Muünker, C. Early Moon formation inferred from hafnium–tungsten systematics. *Nat. Geosci.* **12**, 696–700 (2019).
46. Kruijer, T. S., Archer, G. J. & Kleine, T. No 182W evidence for early Moon formation. *Nat. Geosci.* **14**, 714–715 (2021).
47. Thiemens, M. M. et al. Reply to: No 182W evidence for early Moon formation. *Nat. Geosci.* **14**, 716–718 (2021).
48. Touboul, M., Kleine, T., Bourdon, B., Palme, H. & Wieler, R. Late formation and prolonged differentiation of the Moon inferred from W isotopes in lunar metals. *Nature* **450**, 1206–1209 (2007).
49. Yu, G. & Jacobsen, S. B. Fast accretion of the Earth with a late Moon-forming giant impact. *Proc. Natl. Acad. Sci. USA* **108**, 17604–17609 (2011).
50. Barboni, M. et al. Early formation of the Moon 4.51 billion years ago. *Sci. Adv.* **3**, 1602365 (2017).
51. Papanastassiou, D. A. & Wasserburg, G. J. Rb–Sr study of a lunar dunite and evidence for early lunar differentiates. In *Proc. 6th Lunar Science Conference* Vol. 2, 1467–1489 (Pergamon Press, Inc., New York, 1975).

52. Norman, M. D., Borg, L. E., Nyquist, L. E. & Bogard, D. D. Chronology, geochemistry, and petrology of a ferroan noritic anorthosite clast from Descartes breccia 67215: clues to the age, origin, structure, and impact history of the lunar crust. *Meteor. Planet. Sci.* **38**, 645–661 (2003).
53. Nemchin, A. A. et al. Timing of crystallization of the lunar magma ocean constrained by the oldest zircon. *Nat. Geosci.* **2**, 133–136 (2009).
54. Tera, F. & Wasserburg, G. J. U–Th–Pb systematics in lunar highland samples from the Luna 20 and Apollo 16 missions. *Earth Planet. Sci. Lett.* **17**, 36–51 (1972).
55. Elkins-Tanton, L. T., Burgess, S. D. & Yin, Q. The lunar magma ocean: reconciling the solidification process with lunar petrology and geochronology. *Earth Planet. Sci. Lett.* **304**, 326–336 (2011).
56. Borg, L. E., Connelly, J. N., Cassata, W. S., Gaffney, A. M. & Bizzarro, M. Chronologic implications for slow cooling of troctolite 76535 and temporal relationships between the Mg-suite and the ferroan anorthosite suite. *Geochim. Cosmochim. Acta* **201**, 377–391 (2017).
57. C. Michaut, J. A. Neufeld. Formation of the lunar primary crust from a long-lived slushy magma ocean. *Geophys. Res. Lett.* **49**, e2021GL095408 (2022).
58. Huang, S., Farkaš, J. & Jacobsen, S. B. Calcium isotopic fractionation between clinopyroxene and orthopyroxene from mantle peridotites. *Earth Planet. Sci. Lett.* **292**, 337–344 (2010).
59. Young, E. D., Galy, A. & Nagahara, H. Kinetic and equilibrium mass-dependent isotope fractionation laws in nature and their geochemical and cosmochemical significance. *Geochim. Cosmochim. Acta* **66**, 1095–1104 (2002).
60. Connelly, J. N., Amelin, Y., Krot, A. N. & Bizzarro, M. Chronology of the solar system's oldest solids. *Astrophys. J. Lett.* **675**, 121–124 (2008).

Acknowledgements

We are grateful to NASA Johnson Space Center and the Curation and Analysis Planning Team for Extraterrestrial Materials for providing the Apollo samples, and Dimitri Papanastassiou for providing lunar mineral separates for this study. We thank Claire Nichols and Joe Aslin for careful editorial handling. Finally, we are thankful to Justin I. Simon and three anonymous reviewers for helpful comments. This work was partly founded by NASA Grants NNX12AH65G and NNX15AH66G.

Author contributions

S.B.J. and H.F. defined the project. F.S. conducted Ca-isotope measurements. H.F. performed analysis and modeling, developed the interpretations, and wrote the manuscript with guidance from S.B.J.

Competing interests

The authors declare no competing interests.

Additional information

Supplementary information The online version contains supplementary material available at https://doi.org/10.1038/s43247-023-00974-4.

Correspondence and requests for materials should be addressed to Hairuo Fu.

Peer review information *Communications Earth and Environment* thanks Justin Simon and the other anonymous reviewer(s) for their contribution to the peer review of this work. Primary Handling Editors: Claire Nichols and Joe Aslin. A peer review file is available.

Reprints and permission information is available at http://www.nature.com/reprints

Publisher's note Springer Nature remains neutral with regard to jurisdictional claims in published maps and institutional affiliations.